Structural characteristic correlated to the electronic band gap in MoS_{2}

Shengqi Chu, Changyong Park, and Guoyin Shen

Phys. Rev. B **94**, 020101 — Published 15 July 2016

DOI: 10.1103/PhysRevB.94.020101

A Structural Characteristic Correlated to the Electronic Band Gap in MoS_2

Shengqi Chu,[1,2,*] Changyong Park,[2] and Guoyin Shen[2,*]

[1] *Institute of High Energy Physics, Chinese Academy of Sciences, Beijing 100049, China*

[2] *HPCAT, Geophysical Laboratory, Carnegie Institution of Washington, Argonne, Illinois 60439, USA*

Abstract:

The structural evolution with pressure in bulk MoS_2 has been investigated by high pressure X-ray diffraction using synchrotron radiation. We found that the out-of-plane S-Mo-S bond angle (θ) increases and that in in-plane (ϕ) decreases linearly with increasing pressure across the known semiconducting to metal phase transition, whereas the Mo-S bond length and the S-Mo-S tri-layer thickness display only little change. Extrapolating the experimental result along the in-plane lattice parameter with pressure, the both S-Mo-S bond angles trend to those found in monolayer MoS_2, which manifests as a structural characteristic closely correlating the electronic band gap of MoS_2 to its physical forms and phases, e.g., monolayer as direct band gap semiconductor, multilayer or bulk as indirect band gap semiconductor, and high-pressure (>19 GPa) bulk form as metal. Combined with the effects of bond strength and van der Waals interlayer interactions, the structural correlations between the characteristic bond angle and electronic band gaps are readily extendible to other transition metal dichalcogenide systems (MX_2 where M = Mo, W and X = S, Se, Te).

The layered structure of molybdenum disulfide (MoS_2) consists of S-Mo-S sandwiched tri-layers (generally referred as monolayer) bonded by van der Waals (vdW) inter-layer attractions. In each monolayer, every Mo atoms are covalently bonded by six S atoms forming a trigonal prismatic coordination [Fig. 1(a)]. The strong intra- and weak inter-layer interactions render MoS_2 to be a useful two-dimensional (2D) material [1].

The tunable electronic structure of MoS_2, modulated by several means [2], has drawn much attention. For example, the bulk MoS_2, an indirect gap semiconductor, shows a pressure-induced metallization and structural phase transition from 2Hc to 2Ha [3–5]. When exfoliated to monolayer, the band gap evolves to a direct band gap [6–8]. By applying pressure on the monolayer MoS_2, an increase (blueshift) of the direct gap by 11.7% (or from 1.85 to 2.08 eV) has been reported from photoluminescence measurements [9]. By applying a small uniaxial tensile stress, on the other hand, a strong reduction (redshift) of the direct gap is observed [10–12] on monolayer MoS_2. While it has been well recognized that the nature of monolayer is seemingly responsible for the observed direct band gap [6,8], all these experimental evidences suggest that the band gap is sensitive to strains.

The band structure under strains has been investigated by several theoretical studies using density functional theory (DFT) [13–24]. It has been predicted that the band gap of monolayer MoS_2 will close eventually at either a large compressive or a large tensile strain [13,16], *viz.*, the direct band gap exists only within a small range of limited strains [16,19]. Guo *et al*. [22] and Fan *et al*. [23], using DFT calculations, showed that the S-Mo-S bond angle of bulk MoS_2 increases with increasing pressure. Chang *et al*. [19] and Fan *et al.* [23] pointed out a key role of the bond angle in describing the band gaps of strained monolayer MX_2 (M: Mo, W; X: S, Se) by orbital analysis and first principle simulations, respectively. Despite these efforts in theoretical studies, there still lacks experimental evidence for a characteristic structural origin for the band gap evolution under strains.

In this Letter, we identify structural characteristics that are sensitive to the tunable electronic band structure of MoS_2, based on the experimentally determined structural evolution with pressure. Our results suggest that the S-Mo-S bond angle is the major structural characteristic strongly correlated to the band gap in MoS_2 regardless of its forms (e.g., monolayer, multilayer or bulk) and external conditions (e.g., high pressure, uniaxial tensile stress). Combined with the effects of metal-chalcogenide bond strength and the vdW interlayer interactions, the description of bandgap behavior with this structural characteristic is extended to other transition metal dichalcogenide systems, MX_2 (M=Mo, W; X=S, Se, Te). We suggest that the bond angle parameter may be generally used as a guide for predicting and synthesizing direct band gap materials in the MX_2 system.

MoS_2 powder samples (Sigma-Aldrich) were loaded into a Ø150 μm hole in rhenium gasket in a symmetric diamond anvil cell (DAC) with anvil culet size of 300 μm. Two x-ray diffraction (XRD) runs were carried out at 16-ID-B [25] and 16-BM-D [26] beamlines, respectively, at High Pressure Collaborative Access Team (HPCAT) at the Advanced Phonon Source. The XRD patterns were collected by a Pilatus 1M-F detector for pressures up to 25 GPa at 16-ID-B and by a Mar345 imaging plate for pressures below 10 GPa at 16-BM-D, with helium and a mixture of 4:1 methanol-ethanol used as pressure transmitting media, respectively. The synchrotron x-ray beams were focused to about 5 μm × 5 μm at the full width at half maximum (FWHM) by Kirkpatrick-Baez mirrors. The detector distance and geometry were calibrated using CeO_2 powder standard from NIST. Pressure was remotely controlled through a double-diaphragm device and measured using an online Ruby fluorescence spectrometer [27].

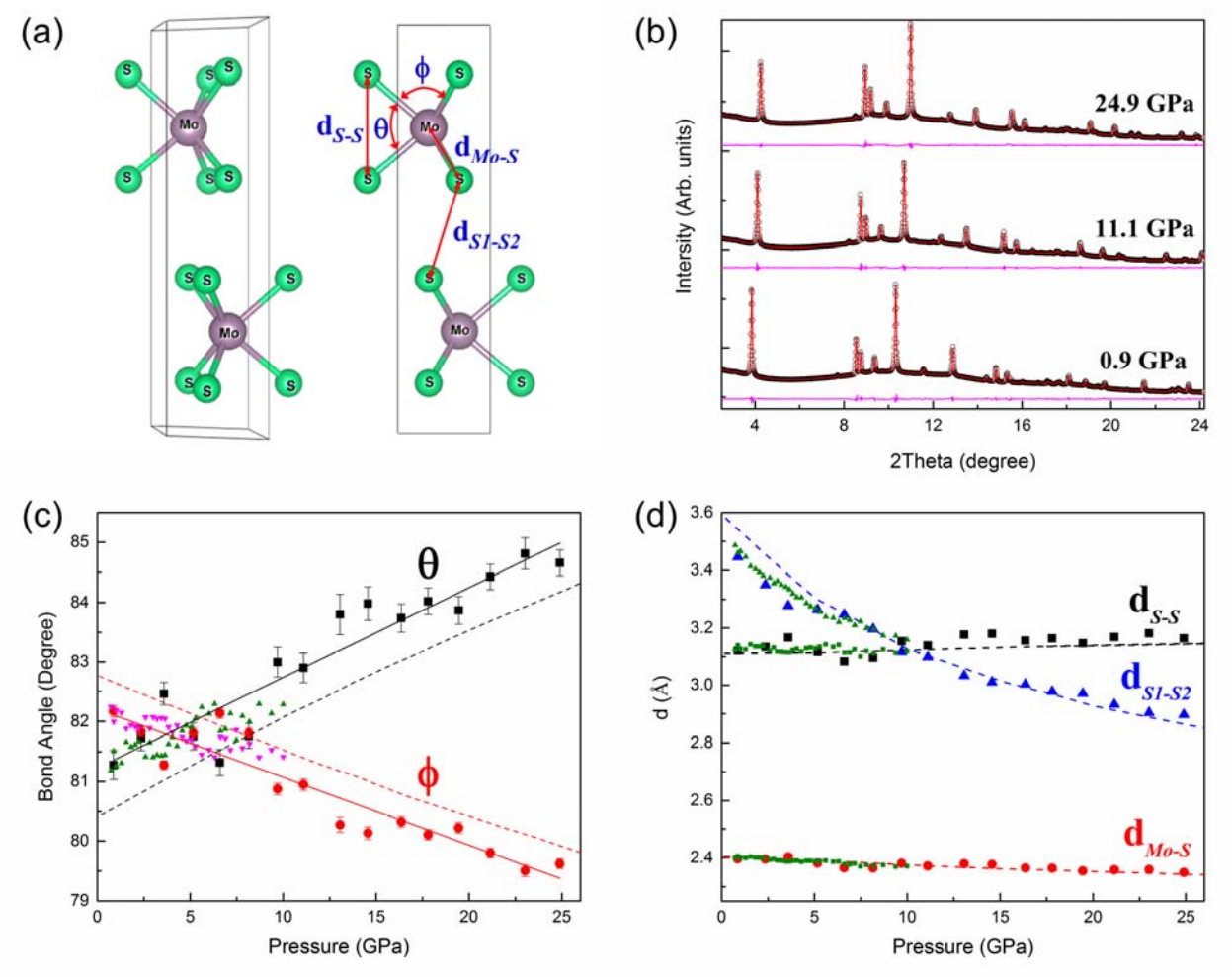

FIG. 1 (color online). (a) The unit cell of MoS_2 in perspective and side views. The definitions of the structural parameters are annotated: θ and ϕ are two S-Mo-S bond angle components forming the trigonal prism coordination, d_{S-S} is S-S bond length in c-axis direction, which is equivalent to the monolayer thickness, d_{Mo-S} is Mo-S bond length, and d_{S1-S2} is the nearest distance of interlayer S atoms. (b) Integrated XRD patterns of three selected pressure points (open black circles). The red and magenta colored lines represent the Rietveld refinement and residuals, respectively. (c) and (d) are pressure dependent variations of the structural parameters denoted in (a). The marked points are our experimental data, and the dashed lines are from the theoretical results of Guo *et al*. [22] for comparison. The solid lines in (c) come from the linear fitting of data points. The big and small markers in (c) and (d) represent the two experimental runs, respectively (see experimental section).

At ambient pressure, the bulk MoS_2 structure belongs to a space group of $P6_3/mmc$ with a stacking order of 2Hc type [Fig. 1(a)]. Our XRD data show no structural transition at pressures up to 25 GPa, which is consistent with the reported high pressure XRD results [3–5]. We performed Rietveld refinement to

obtain detailed structural characteristics from the measured high quality XRD patterns [Fig. 1(b) and Fig. S1]. It is found that the bond angle θ [Fig. 1(a)] increases, while ϕ [Fig. 1(a)] decreases, both linearly with increasing hydrostatic pressure [Fig. 1(c)]. The distinct linear trends in the opposite directions are consequences of reduction in Mo-S ($d_{Mo\text{-}S}$) bond length and expansion of monolayer thickness ($d_{S\text{-}S}$) with increasing pressure [Fig. 1(d)]. The change in Mo-S bond length is about 3 times smaller than that in in-plane lattice parameter (*a*) due to the strong covalent bonding between Mo and S atoms, which causes the increase in the monolayer thickness ($d_{S\text{-}S}$) and leads to the systematic increase in θ and the decrease in ϕ. The changes in θ and ϕ are qualitatively in agreement with those from theoretical calculations [22,23] [dashed lines in Fig.1 (c) and (d)], although there is a distinct offset due to the different initial lattice parameters used in the theoretical calculations, especially the atomic position parameters of S atoms (shown in Fig. S2). In contrast to the relatively small changes in $d_{S\text{-}S}$ and $d_{Mo\text{-}S}$, the interlayer distance ($d_{S1\text{-}S2}$) decreases significantly and non-linearly with increasing pressure due to the weak vdW interlayer interaction [Fig. 1(d)].

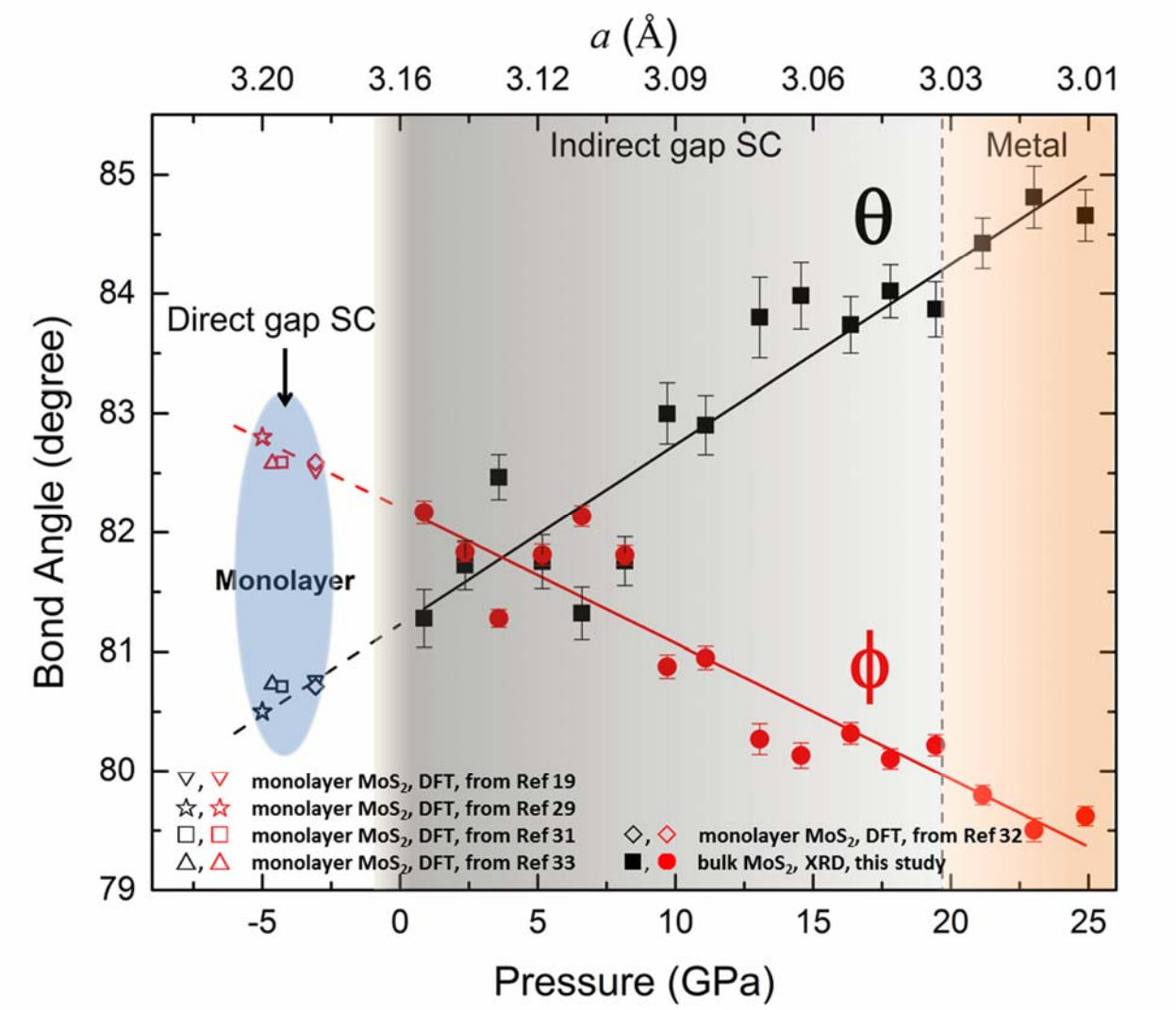

FIG. 2 (color online). Correlations of electronic band gap properties with the observed bond angles with pressure in MoS_2. The filled symbols with error bars are from our XRD experiments; the solid lines are the linear regressions. The dashed lines are extrapolations of the fitted lines to a negative pressure. The open symbols in the negative pressure regime are the bond angles of monolayer MoS_2 from previous theoretical works [19,29,31–33]. The negative pressure values for each data point correspond to the in-plane lattice parameter *a* (top axis).

Figure 2 expresses the correlation of electronic band gap properties with the observed bond angle variations with pressure. The pressure-induced metallization in bulk MoS_2 as experimentally determined occurs at about 19 GPa [3]. Based on the linear fitting of our experimental data (Fig. 1(c) and Fig. 2), the

θ (ϕ) angle at this phase transition pressure equals to ~84.1° (~80.0°), which corresponds to the bond angle values at 25 GPa predicted for the same phase transition by Guo *et al*. [22]. This indicates a characteristic role of bond angles in describing the electronic structure of MoS_2.

Based on the distinct linearity in bond angle variations with pressure, we extrapolate the trend to a fictive negative pressure regime to represent a scenario with expanded lattice parameters. Bulk MoS_2 can be mechanically exfoliated to a 2D monolayer [28]. For the monolayer MoS_2, a recent calculation by Huang *et al*. [29] gives the values of θ and ϕ as 80.5 and 82.8, respectively (open pentagrams in Fig 2), which coincide with the extended linear lines to the negative pressure range at about -5 GPa. As there are two degrees of freedom (i.e., the absolute values for each and the relative difference between them), the determination of matching pressure is non-trivial and thus confirms the universal trend that θ increases, and ϕ decreases, linearly with increasing pressure or *vice versa* over the extended pressure ranges. Based on this consistency, other structural parameters can be estimated by fitting the experimental data with setting of P = -5 GPa (listed in Table S1). The in-plane lattice parameter (*a*) of monolayer MoS_2 is found to be expanded about ~1% with respect to the bulk (from 3.161 Å to 3.196 Å), which agrees well with the calculated result of Huang *et al.* [29]. ~~Although the negative pressure is not practical,~~ It is remarkable that the trend predicted by its hypothetical extension coincide with the effect expected from mechanical exfoliation of MoS_2.

Several other theoretical studies have reported the expansion of *a* parameter and the decrease in θ of monolayer MoS_2 based on the structure optimization by DFT (open symbols in Fig.2 and details listed in Table S2) [13,19,20,29–33]. Because of the lack of experimental evidence, it has been surmised [19,23,29,30] that this lateral expansion might be attributed to an overestimation in the computational models. On the other hand, there exist several experimental studies that imply the expansion of *a* and the decrease in θ of monolayer MoS_2. Jin *et al.* [34] reported 3.6 % expansion of the

in-plane lattice for monolayer MoS_2 using angle-resolved photoemission spectroscopy (ARPES), although this 3.6% expansion may be likely overestimated, because this would yield a lattice parameter of 3.28 Å and cause the monolayer MoS_2 to be metastable with distorted octahedral coordination (i.e., 1T-MoS_2) [35]. The surface structure of cleaved MoS_2 crystals under ultrahigh vacuum condition [36,37] showed that the intraplanar distance between the top S plane and the middle Mo plane are contracted by a few percent compared to the bulk value leading to a reduced θ angle. Another important experimental observation indirectly indicating the decrease in θ angle is the "anomalous" blue shift of the frequency of E^1_{2g} Raman mode as the number of layers decreases from the bulk to the 2D limit, i.e., the monolayer [38]. The E^1_{2g} mode originates from the in-plane vibration of two S atoms opposed to the Mo atom [30,39,40]. With a minimal change in the Mo-S bond length, a reduction in θ angle will lead to an increase of the in-plane component of the Mo-S bond strength, stiffening the E^1_{2g} vibration as observed.

In Fig. 2, we show that all of the theoretically predicted bond angles for monolayer MoS_2 [19,29,31–33] fall onto the negative pressure regime. In other words, the θ angle increases from monolayer to bulk due to the vdW interlayer interactions. And for the bulk MoS_2, this trend continues linearly with increasing pressure based on our experimental results. Combined with the known electronic band structures of MoS_2, e.g., monolayer as direct band gap semiconductor, multilayer or bulk as indirect band gap semiconductor, and high-pressure (>19 GPa) bulk form as metal (Fig. 2), our results suggest that the flexible S-Mo-S bond angles show strong correlations with the electronic band gap properties of MoS_2 regardless of its forms (monolayer, multilayers, or bulk) and environmental conditions (compression or tensile stress).

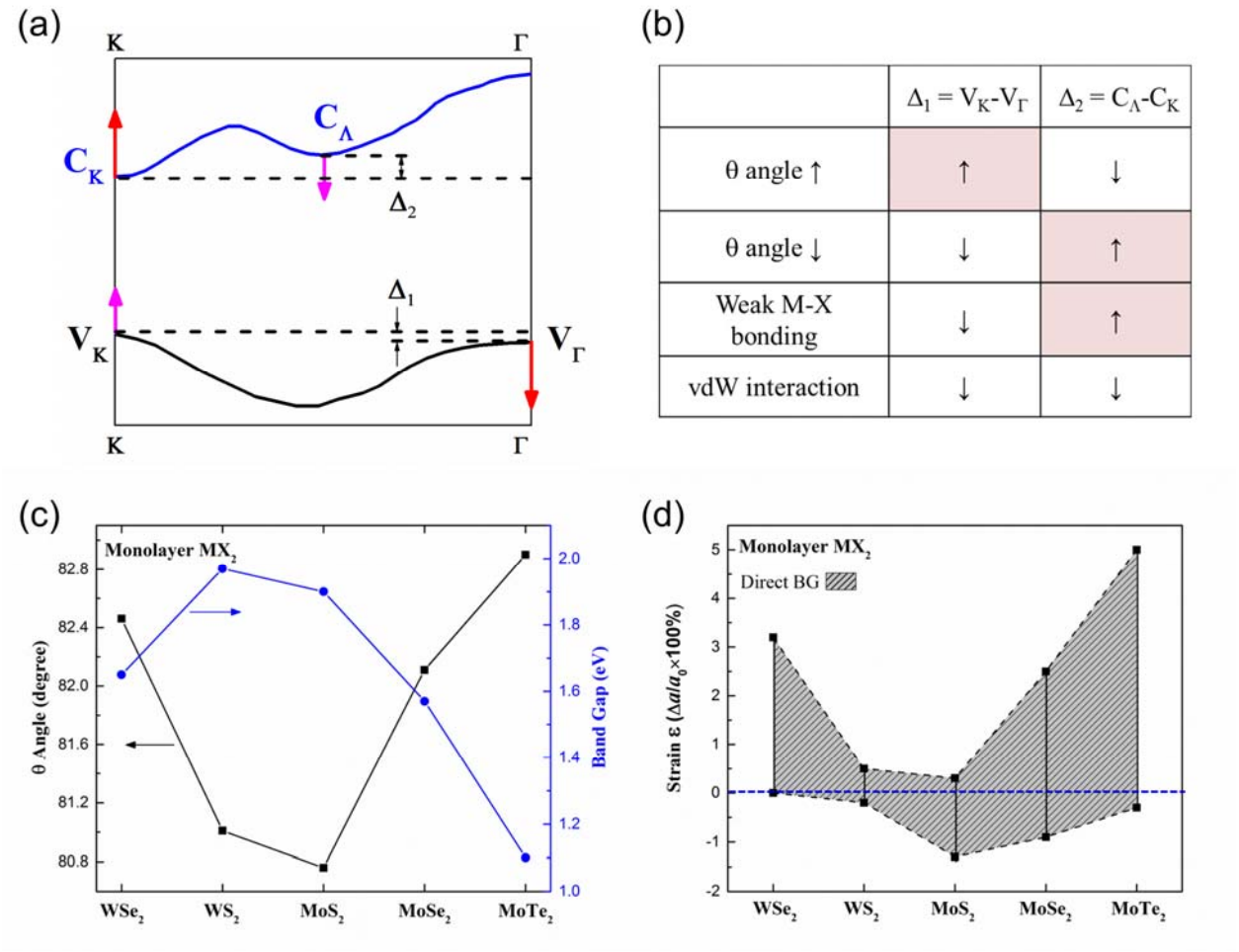

FIG. 3 (color online). (a) Schematic of electronic band map of monolayer MoS_2 along the K-Γ high symmetry line. Black and blue solid lines are the top of valence band and the bottom of conduction band, respectively. Colored arrows indicate change in directions of the four main features when θ angle increases. (b) List of factors influencing the energy differences Δ_1 and Δ_2, defined in (a). The ↑ and ↓ symbols represent the increase and decrease of the values, respectively. The highlighted areas show the beneficial conditions to increase Δ_1 or Δ_2 in order to retain the direct band gap. (c) θ angle, calculated by Chang *et al*. [19], and experimental band gaps of monolayer MX_2 [6,7,41-43]. The arrows indicate the corresponding axes. (d) The range of strain as defined by $\Delta a/a_0$ for monolayer MX_2 to retain the direct band gap, calculated by Yun *et al*. [16]. The blue dashed line shows the zero-strain state.

To better understand the correlation between the bond angle and the band gap behavior, we consider several factors affecting the band structure of monolayer MoS_2. Fig. 3(a) illustrates the main features of the MoS_2 band structure based on DFT calculations [14,16,19] and ARPES measurements [8]. There are

two peaks at top of valence band located at K and Γ points, respectively (denoted as V_K and V_Γ), and two valleys at bottom of conduction band located at K and midpoint of K- Γ line, respectively (denoted as C_K and C_Λ). These four features are divided into two groups according to the anisotropy in the structure. The energy gaps at V_Γ and C_K depend on the degrees of overlap of the out-of-plane orbitals (Mo d_{z^2} and S p_z) and can be considered as a split of the bonding-antibonding state [15]. On the other hand, V_K and C_Λ originates from the coupling of the in-plane orbitals (Mo d_{xy}, $d_{x^2-y^2}$ and S p_x, p_y). The conduction band minimum and the valence band maximum coincide at the K point in monolayer MoS_2, making it a direct band gap semiconductor. With increasing pressure, the bond angle θ will increase (Fig. 2), resulting in a stronger coupling of the out-of-plane orbitals and a weaker interaction for the in-plane orbitals. Consequently, the energy splitting between V_Γ and C_K becomes larger and that between V_K and C_Λ gets closer to each other, as shown by the arrows in Fig. 3(a). In addition, because θ angle has a stronger effect on the out-of-plane interaction and a weaker effect on the in-plane bonding [8,19], the changes in the band energy, respectively, are different as indicated by the length of arrows in Fig. 3(a). Along this trend, the band gap of monolayer MoS_2 increases first because the C_K changes faster than the V_K, and then reach a maximum while retaining the direct gap, which has been demonstrated by photoluminescence measurements under high pressure [9]. Eventually, the V_K-C_Λ gap becomes smaller, leading to a crossover from K-K direct to Λ-K indirect gap. Upon decreasing pressure, on the other hand, the four features in the band structure all move in the opposite directions as θ will decrease. The direct band gap reduces first and then turns into K-Γ indirect gap. Therefore, the direct band gap exists only within a certain range of S-Mo-S bond angle by this mechanism.

Interestingly, it is found that all monolayer materials in the other transition metal dichalcogenides, MX_2 (M=Mo, W; X=S, Se, Te), are direct gap semiconductors, but with interesting systematic trends among them. For example, the direct band gap of monolayer MX_2 decreases from MoS_2 (1.9 eV) [6,7], $MoSe_2$ (1.57 eV) [41] to $MoTe_2$ (1.10 eV) [42], whereas it increases from MoS_2 to WS_2 (1.97 eV) [43]. Fig. 3(c) shows their θ angles and direct band gaps. From MoS_2 to WS_2, the θ angle increases only 0.3% owing to the similar atomic radii of Mo and W (Table S3). The band gap then should increase, which is consistent with the experimental results [43]. However, for $MoSe_2$, the θ angle becomes much larger (1.7%) than that of MoS_2. By a simple extrapolating from the above analysis, it would suggest $MoSe_2$ turning into an indirect gap semiconductor, which does not conform to the experimental observation [41]. This may be explained by the weaker Mo-Se bonding because of the longer bond length and more delocalized 4p orbitals of Se. In general, a weaker M-X bonding will reduce the both in-plane and out-of-plane interactions and decreases the overall band gap eventually. From WS_2 to WSe_2, the direct band gap also decreases following the same reason. Note that the V_Γ and C_K change faster than V_K and C_Λ [8,19], which causes the increase of Δ_1 (= V_K - V_Γ) and the decrease of Δ_2 (= C_Λ - C_K) with increase of θ angle [Fig. 3(b)]. Combining the effect of weaker M-X bonding and increasing θ angle, along the trend of MoS_2, $MoSe_2$ to $MoTe_2$, the relative change in Δ_1 will be larger than that in Δ_2 , which is consistent with previous DFT calculations and experimental results [8,44–46]. Similarly, the direct band gap decreases following the trend (Fig. 3(c)). The change in Δ_1 and Δ_2 determines the nature of the band gap in monolayer MX_2, such as retaining the direct band gap requires both of them to be positive. In Fig. 3(d), the range of strain to fulfil this condition is expressed based on the structures and band gaps reported for monolayer MX_2 [16].

Finally, from monolayer to bulk, V_Γ will rise and C_Λ will drop with increasing vdW interlayer interaction [8,14,16,47,48], thus resulting in indirect gap for all bulk MX_2 systems. Under high pressure

conditions, the vdW interaction becomes stronger due to the reduced interlayer spacing [Fig. 1(d)], which will accelerate the metallization in bulk materials as compared to the monolayer counterparts [9]. On the other hand, high temperature is likely to weaken the coupling of neighboring layers via interlayer thermal expansion, which may drive a crossover from indirect to direct band gap as seen in few-layer $MoSe_2$ [49].

In summary, the pressure-induced structural changes in bulk MoS_2 have been refined, showing that the out-of-plane S-Mo-S bond angle θ increases and in-plane bond angle ϕ decreases linearly with increasing pressure. The bond angles are found to have strong correlations with the electronic band structures of MoS_2 and other similar MX_2 systems with a remarkable consistency over a variety of forms (e.g., monolayer and bulk) and environments (e.g., high pressure and tensile stress). For the conditions to retain the direct band gap, the effects of X-M-X bond angle, M-X bond strength and vdW interlayer interaction were combined to establish a consistent view across the various different MX_2 systems. Considering these factors affecting the band gaps, it may be possible to realize the direct band gap in multilayer MX_2 or even bulk materials, e.g., through weakening the M-X bonding, heating, or modulating the θ angle by strains, which provides guides for predicting and synthesizing novel materials for future optoelectronic applications. In addition, our results open a new way to investigate the strain-related structural variation of 2D materials by probing the bulk counterparts.

Acknowledgement:

This work is supported by DOE grants of DE-NA0001974 and DE-FG02-99ER45775. We thank Curtis Kenney-Benson, Ligang Bai, Chuanlong Lin and Rui Li for their technical assistance, and S. N. Tkachev for

the assistance in gas loading. HPCAT operations are supported by DOE-NNSA under Award No. DE-NA0001974 and DOE-BES under Award No. DE-FG02-99ER45775, with partial instrumentation funding by NSF. The Advanced Photon Source is a U.S. Department of Energy (DOE) Office of Science User Facility operated for the DOE Office of Science by Argonne National Laboratory under Contract No. DE-AC02-06CH11357. SC acknowledges the support from the visiting scholar project funded by China Scholarship Council, and the Natural Science Foundation of China (Grant No. 11305199). The COMPRES-GSECARS gas loading systems was supported by COMPRES under NSF Cooperative Agreement EAR-1157758 and by GSECARS through NSF grant EAR-1128799 and DOE grant DE-FG02-94ER14466.

*Corresponding authors: chusq@ihep.ac.cn, gshen@ciw.edu

References:

[1] R. Ganatra and Q. Zhang, ACS Nano **8**, 4074 (2014).

[2] H. Wang, H. Yuan, S. Sae Hong, Y. Li, and Y. Cui, Chem. Soc. Rev. **44**, 2664 (2015).

[3] A. P. Nayak, S. Bhattacharyya, J. Zhu, J. Liu, X. Wu, T. Pandey, C. Jin, A. K. Singh, D. Akinwande, and J.-F. Lin, Nat. Commun. **5**, 3731 (2014).

[4] Z.-H. Chi, X.-M. Zhao, H. Zhang, A. F. Goncharov, S. S. Lobanov, T. Kagayama, M. Sakata, and X.-J. Chen, Phys. Rev. Lett. **113**, 036802 (2014).

[5] N. Bandaru, R. S. Kumar, D. Sneed, O. Tschauner, J. Baker, D. Antonio, S.-N. Luo, T. Hartmann, Y. Zhao, and R. Venkat, J. Phys. Chem. C **118**, 3230 (2014).

[6] K. F. Mak, C. Lee, J. Hone, J. Shan, and T. F. Heinz, Phys. Rev. Lett. **105**, 136805 (2010).

[7] A. Splendiani, L. Sun, Y. Zhang, T. Li, J. Kim, C.-Y. Chim, G. Galli, and F. Wang, Nano Lett. **10**, 1271 (2010).

[8] W. Jin, P.-C. Yeh, N. Zaki, D. Zhang, J. T. Sadowski, A. Al-Mahboob, A. M. van der Zande, D. A. Chenet, J. I. Dadap, I. P. Herman, P. Sutter, J. Hone, and R. M. Osgood, Phys. Rev. Lett. **111**, 106801 (2013).

[9] A. P. Nayak, T. Pandey, D. Voiry, J. Liu, S. T. Moran, A. Sharma, C. Tan, C.-H. Chen, L.-J. Li, M. Chhowalla, J.-F. Lin, A. K. Singh, and D. Akinwande, Nano Lett. **15**, 346 (2015).

[10] H. J. Conley, B. Wang, J. I. Ziegler, R. F. Haglund, S. T. Pantelides, and K. I. Bolotin, Nano Lett. **13**, 3626 (2013).

[11] K. He, C. Poole, K. F. Mak, and J. Shan, Nano Lett. **13**, 2931 (2013).

[12] C. R. Zhu, G. Wang, B. L. Liu, X. Marie, X. F. Qiao, X. Zhang, X. X. Wu, H. Fan, P. H. Tan, T. Amand, and B. Urbaszek, Phys. Rev. B **88**, 121301 (2013).

[13] E. Scalise, M. Houssa, G. Pourtois, V. Afanas'ev, and A. Stesmans, Nano Res. **5**, 43 (2012).

[14] T. Cheiwchanchamnangij and W. R. L. Lambrecht, Phys. Rev. B **85**, 205302 (2012).

[15] Q. Yue, J. Kang, Z. Shao, X. Zhang, S. Chang, G. Wang, S. Qin, and J. Li, Phys. Lett. A **376**, 1166 (2012).

[16] W. S. Yun, S. W. Han, S. C. Hong, I. G. Kim, and J. D. Lee, Phys. Rev. B **85**, 033305 (2012).

[17] L. Hromadová, R. Martoňák, and E. Tosatti, Phys. Rev. B - Condens. Matter Mater. Phys. **87**, 1 (2013).

[18] W. Zhao, R. M. Ribeiro, M. Toh, A. Carvalho, C. Kloc, A. H. Castro Neto, and G. Eda, Nano Lett. **13**, 5627 (2013).

[19] C.-H. Chang, X. Fan, S.-H. Lin, and J.-L. Kuo, Phys. Rev. B **88**, 195420 (2013).

[20] A. Kumar and P. K. Ahluwalia, Phys. B Condens. Matter **419**, 66 (2013).

[21] H. Shi, H. Pan, Y.-W. Zhang, and B. I. Yakobson, Phys. Rev. B **87**, 155304 (2013).

[22] H. Guo, T. Yang, P. Tao, Y. Wang, and Z. Zhang, J. Appl. Phys. **113**, 013709 (2013).

[23] X. Fan, C.-H. Chang, W. T. Zheng, J.-L. Kuo, and D. J. Singh, J. Phys. Chem. C **119**, 10189 (2015).

[24] S. Bhattacharyya, T. Pandey, and A. K. Singh, Nanotechnology **25**, 465701 (2014).

[25] J. S. Smith, S. V Sinogeikin, C. Lin, E. Rod, L. Bai, and G. Shen, Rev. Sci. Instrum. **86**, 072208 (2015).

[26] C. Park, D. Popov, D. Ikuta, C. Lin, C. Kenney-Benson, E. Rod, A. Bommannavar, and G. Shen, Rev. Sci. Instrum. **86**, 072205 (2015).

[27] S. V Sinogeikin, J. S. Smith, E. Rod, C. Lin, C. Kenney-Benson, and G. Shen, Rev. Sci. Instrum. **86**, 072209 (2015).

[28] K. S. Novoselov, D. Jiang, F. Schedin, T. J. Booth, V. V Khotkevich, S. V Morozov, and A. K. Geim, Proc. Natl. Acad. Sci. U. S. A. **102**, 10451 (2005).

[29] L. F. Huang, P. L. Gong, and Z. Zeng, Phys. Rev. B **90**, 045409 (2014).

[30] C. Ataca, M. Topsakal, E. Aktürk, and S. Ciraci, J. Phys. Chem. C **115**, 16354 (2011).

[31] Y. Ding, Y. Wang, J. Ni, L. Shi, S. Shi, and W. Tang, Phys. B Condens. Matter **406**, 2254 (2011).

[32] A. Ramasubramaniam, Phys. Rev. B **86**, 115409 (2012).

[33] Z. Y. Zhu, Y. C. Cheng, and U. Schwingenschlögl, Phys. Rev. B **84**, 153402 (2011).

[34] W. Jin, P.-C. Yeh, N. Zaki, D. Zhang, J. T. Liou, J. T. Sadowski, A. Barinov, M. Yablonskikh, J. I. Dadap, P. Sutter, I. P. Herman, and R. M. Osgood, Phys. Rev. B **91**, 121409 (2015).

[35] D. Yang, S. J. Sandoval, W. M. R. Divigalpitiya, J. C. Irwin, and R. F. Frindt, Phys. Rev. B **43**, 12053 (1991).

[36] B. J. Mrstik, R. Kaplan, T. L. Reinecke, M. Van Hove, and S. Y. Tong, Phys. Rev. B **15**, 897 (1977).

[37] Y. Kadowaki, K. Aika, H. Kondoh, and H. Nozoye, Surf. Sci. **287-288**, 396 (1993).

[38] C. Lee, H. Yan, L. E. Brus, T. F. Heinz, J. Hone, and S. Ryu, ACS Nano **4**, 2695 (2010).

[39] H. Li, Q. Zhang, C. C. R. Yap, B. K. Tay, T. H. T. Edwin, A. Olivier, and D. Baillargeat, Adv. Funct. Mater. **22**, 1385 (2012).

[40] X. Luo, Y. Zhao, J. Zhang, Q. Xiong, and S. Y. Quek, Phys. Rev. B **88**, 075320 (2013).

[41] P. Tonndorf, R. Schmidt, P. Böttger, X. Zhang, J. Börner, A. Liebig, M. Albrecht, C. Kloc, O. Gordan, D. R. T. Zahn, S. Michaelis de Vasconcellos, and R. Bratschitsch, Opt. Express **21**, 4908 (2013).

[42] C. Ruppert, O. B. Aslan, and T. F. Heinz, Nano Lett. **14**, 6231 (2014).

[43] W. Zhao, Z. Ghorannevis, L. Chu, M. Toh, C. Kloc, P.-H. Tan, and G. Eda, ACS Nano **7**, 791 (2013).

[44] I. G. Lezama, A. Ubaldini, M. Longobardi, E. Giannini, C. Renner, A. B. Kuzmenko, and A. F. Morpurgo, 2D Mater. **1**, 021002 (2014).

[45] Y. Zhang, T.-R. Chang, B. Zhou, Y.-T. Cui, H. Yan, Z. Liu, F. Schmitt, J. Lee, R. Moore, Y. Chen, H. Lin, H.-T. Jeng, S.-K. Mo, Z. Hussain, A. Bansil, and Z.-X. Shen, Nat. Nanotechnol. **9**, 111 (2014).

[46] T. Böker, R. Severin, A. Müller, C. Janowitz, R. Manzke, D. Voß, P. Krüger, A. Mazur, and J. Pollmann, Phys. Rev. B **64**, 235305 (2001).

[47] A. Kuc, N. Zibouche, and T. Heine, Phys. Rev. B **83**, 245213 (2011).

[48] A. Ramasubramaniam, D. Naveh, and E. Towe, Phys. Rev. B **84**, 205325 (2011).

[49] S. Tongay, J. Zhou, C. Ataca, K. Lo, T. S. Matthews, J. Li, J. C. Grossman, and J. Wu, Nano Lett. **12**, 5576 (2012).